Materials Chemistry and Physics 190 (2017) 166–174

Contents lists available at ScienceDirect

Materials Chemistry and Physics

journal homepage: www.elsevier.com/locate/matchemphys

Influence of synthesis time on the microstructure and photophysical properties of Gd-MOFs doped with Eu^{3+}

Jarley Fagner Silva do Nascimento [a, d], Bráulio Silva Barros [a, b, *], Joanna Kulesza [c], João Bosco Lucena de Oliveira [a], Ana Karina Pereira Leite [a], Rosivânia Silva de Oliveira [a]

[a] Federal University of Rio Grande do Norte, Institute of Chemistry, PO Box 1662, 59078-970, Natal, RN, Brazil
[b] Federal University of Pernambuco, Department of Mechanical Engineering, 50070-901, Recife, PE, Brazil
[c] Federal University of Pernambuco, Department of Fundamental Chemistry, 50070-901, Recife, PE, Brazil
[d] Federal Institute of Education, Science and Technology of the Rio Grande do Norte, 59500-000, Macau, RN, Brazil

HIGHLIGHTS

- Red-luminescent Eu/Gd-1,4BDC MOFs were obtained by solvothermal method.
- Efficient antenna effect was observed.
- PL properties were morphology dependent.

GRAPHICAL ABSTRACT

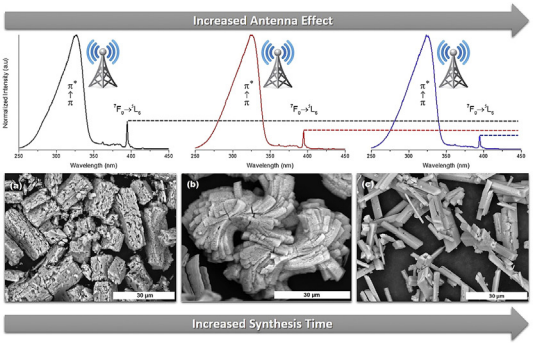

ARTICLE INFO

Article history:
Received 12 October 2016
Received in revised form
23 December 2016
Accepted 8 January 2017
Available online 9 January 2017

Keywords:
MOFs
Lanthanides
Antenna effect
Photoluminescence
Microstructure

ABSTRACT

Metal Organic Frameworks (MOFs) are hybrid materials, usually crystalline, consisting of metallic species or clusters, connected by polytopic organic ligands originating bi or tridimensional porous structures. In this work, Gd-1,4-BDC-MOFs doped with 5% mol Eu^{3+} were synthesized via solvothermal method at 180 °C. The effect of the synthesis time (3, 5 or 7 days) on the microstructure and photophysical properties of the obtained MOFs were evaluated. It was found that porous agglomerates were formed within three days, gradually changing their morphology to rod-like crystals within seven days. The photoluminescence excitation and emission spectra revealed an efficient energy transfer from the ligand to the Eu^{3+} levels (antenna effect), what is not expected for 1,4-BDC^{2-} in a Eu(III)-based MOFs. We concluded that the presence of highly paramagnetic Gd^{3+} ions in the matrix enhanced the antenna effect, resulting in a strong red emission.

1. Introduction

Metal-organic frameworks (MOFs) comprise a broad class of crystalline materials defined as porous networks consisting of metallic ions or clusters linked together by organic multidentate

* Corresponding author. Federal University of Pernambuco, Department of Mechanical Engineering, Av. Prof. Moraes Rego-1235 – Cidade Universitária, 50070-901, Recife, PE, Brazil.
E-mail address: braulio.barros@ufpe.br (B.S. Barros).

http://dx.doi.org/10.1016/j.matchemphys.2017.01.024
0254-0584/

ligands [1]. Due to their well-defined crystallinity and porosity, high stability and versatility of structures and topologies, these materials have attracted considerable attention in the past two decades [2,3].

More recently, MOFs containing lanthanide ions, so-called LOFs (Lanthanide-Organic Frameworks) have received growing attention due to the unique properties of lanthanide ions [4–8] combined with the fascinating structural diversity of MOFs.

The potential applications of these materials are very diverse. They can be used as light-emitting materials, sensors [7,9,10], multimodal imaging contrast agents [11], catalysts [12], drug delivery carriers [13,14] and markers for gunshot residues [15,16].

Among different organic linkers used for the preparation of LOFs, aromatic carboxylic acids are preferred as they induce rigidity and porosity to a framework [17]. Moreover, considering a lack of the preferential geometry of lanthanide ions, carboxylate groups with their diversity of coordination modes, are good candidates for formation of LOFs. Linear linkers such as terephthalic acid (1,4 - H_2BDC) can be considered as an ideal organic binder. It usually promotes the growth of network homogeneously and acts as a bridge between metal centers leading to a great variety of structures [17,18]. Several examples of LOFs based on 1,4 − BDC have been revealed [19–23].

Although the luminescent properties of Eu-1,4-BDC-MOFs have already been reported [24], little attention has been paid to investigate the relationship between the morphology of obtained LOFs and their photophysical properties. Since properties such as photoluminescence, depend directly on structural and morphological characteristics of materials, it is crucial to understand a mechanism of self-assembly and agglomeration of LOFs particles [3,24]. Moreover, to the best of our knowledge, Gd-1,4-BDC-MOFs doped with Eu^{3+} have never been described before.

Thus, this study aims to evaluate the effect of the synthesis time on the microstructure and photophysical properties of Gd/Eu-MOFs of the general formula $[Gd_{1.9}Eu_{0.1}(1,4\text{-BDC})_3(DMF)_2(H_2O)]_n$.

2. Experimental section

2.1. Materials and methods

All reagents and solvents were used as received without further purification. Terephthalic acid (1,4-H_2BDC), gadolinium oxide Gd_2O_3 and europium oxide Eu_2O_3 were purchased from Sigma Aldrich. *N,N*-dimethylformamide (DMF), ethanol (EtOH) and nitric acid (HNO_3, 65%) were acquired from Vetec.

2.2. Synthesis of Eu-doped Gd-MOFs

Gd-MOFs doped with Eu^{3+} were prepared as follows: stoichiometric amounts of gadolinium (Gd_2O_3) and europium (Eu_2O_3) oxides, 0.19 mmol and 0.01 mmol, respectively, were dissolved in an aqueous solution of HNO_3 and kept under constant stirring at 70 °C until complete solvent evaporation. Subsequently, to generated *in situ* lanthanide nitrates, 10 ml of DMF solution containing 1.6 mmol of 1,4 − H_2BDC were added under constant stirring at room temperature. The resulting solution was placed in a 23 mL Teflon-lined steel reactor and heated in an oven at 180 °C for 3, 5 or 7 days, respectively. Next, the mixture was cooled down to room temperature, and the obtained white solid was filtered, washed with DMF and EtOH and dried at 60 °C for 24 h. Three samples of a general formula ($[Gd_{1.9}Eu_{0.1}(1,4\text{-BDC})_3(DMF)_2(H_2O)]_n$) prepared within different synthesis time (3, 5 and 7 days), were then characterized and studied. For comparison, undoped sample Gd-1,4-BDC was also prepared according to the similar synthetic procedure.

2.3. Sample characterizations

Powder X-ray diffraction (PXRD) data were recorded on a Bruker D2 Phaser diffractometer using Cu Kα radiation (λ = 1.5406 Å) with a Ni filter, operating at 30 kV and 10 mA. The PXRD patterns were recorded between 5 and 50° at steps of 0.02°. Simulated from single crystal data PXRD patterns were calculated using the program Mercury 3.7.

Thermogravimetric analyses (TGA) were performed on a Shimadzu DTG-60H thermal analysis system. Samples were heated from 30 °C to 900 °C at a rate of 20 °C/min under nitrogen atmosphere. Attenuated total reflection Fourier transform infrared (ATR-FTIR) experiments were carried out on a Bruker Vertex 70/v spectrometer. Morphological analysis of powders was performed on Scanning Electron Microscopy (SEM) in a Hitachi Tabletop Microscope equipment with 5 kV acceleration, TM model 3000. The excitation and emission spectra were collected in a solid state at 298 K on a Fluorolog3 Horiba Jobin Yvon spectrofluorometer equipped with Hamamatsu R928P photomultiplier, SPEX 1934 D phosphorimeter, and a pulsed 150 W Xe-Hg lamp.

3. Results and discussion

3.1. Sample characterization

The XRD patterns of the Eu/Gd-MOF powders obtained within different synthesis times are shown in Fig. 1. These diffractograms coincide with a pattern of the Gd-MOF sample previously prepared by the same route, suggesting that europium has no specific role in the crystallization process. It can be observed that the sample prepared within three days showed very low crystallinity compared to other samples, indicating that a longer time of reaction is needed for producing highly crystalline materials.

All analyzed patterns match well with the simulated pattern from the single-crystal structure of $[Eu_2(BDC)_3(DMF)_2(H_2O)\cdot DMF]$, previously reported by Decadt and co-workers [24]. As the authors described, this structure was solved at a low-temperature experiment (100 K), what justifies the peak shift observed in comparison to experimental XRD data collected from powder at room temperature. Because the ionic radii of Eu^{3+} and Gd^{3+} are comparable (1.07 Å and 1.05 Å, respectively), Eu^{3+} ions can substitute Gd^{3+} ions without any significant changes in the crystal structure. However, it is worth to note that the intensity ratio between the diffraction peaks at 9.4 and 9.7° (2θ), assigned to the crystal planes (10-1) and (01-1), respectively, is smaller in the simulated pattern when compared to the experimental patterns. A second simulated pattern, also shown in Fig. 1, was calculated without considering DMF molecules in the pores. In this case, the intensity ratio between the diffraction peaks at 9.4 and 9.7° is quite similar to the intensity ratio observed in the experimental patterns, suggesting the absence of non-coordinated solvent molecules in the structure.

The crystal structure contains two binuclear inorganic building blocks, in both cases, trivalent lanthanides (Ln^{3+}) centers are octacoordinated in a distorted square antiprism geometry (Fig. 2). In the first building block type, each Ln^{3+} center is coordinated to six oxygen atoms from carboxylate groups and two from DMF and water molecules, respectively. In the second type, each Ln^{3+} center also has eight oxygen atoms, seven from carboxylate groups and one oxygen atom from a DMF molecule. These two building blocks are connected by carboxylate groups from two different 1,4-BDC^{2-} ligands, forming 1D chains. The chains are cross-linked by 1,4-BDC^{2-} ligands resulting in a 3D structure with porous channels along the crystallographic direction [111] (Fig. 3).

Fig. 4 presents the FTIR spectra of Gd/Eu-MOF samples prepared within different synthesis times, as well as, of 1,4-H_2BDC and DMF.

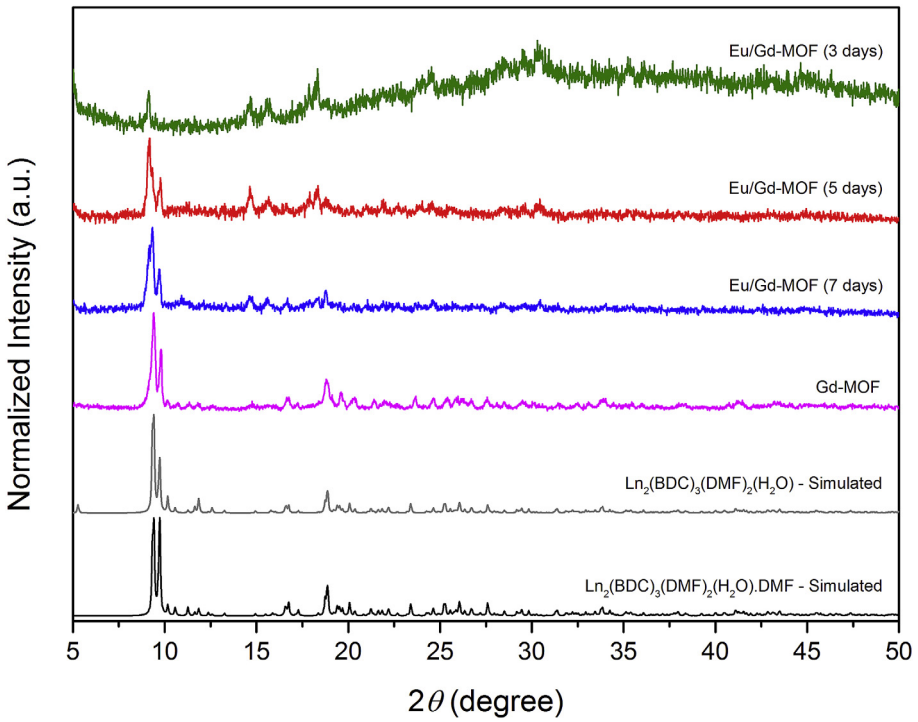

Fig. 1. PXRD patterns of the synthesized Eu/Gd-MOF samples (prepared within different synthesis time - 3, 5 and 7 days) and of the pure Gd-MOF matrix, in comparison with the simulated from single crystal data PXRD patterns of $Eu_2(BDC)_3(DMF)_2(H_2O)$ and $Eu_2(BDC)_3(DMF)_2(H_2O)\cdot DMF$.

In the IR spectra of MOF samples, no band at 1670 cm^{-1} corresponding to the COOH groups is present, indicating the complete deprotonation of the carboxylic acid and coordination of COO^- groups to the metal center. The bands in the region between 1584 and 1503 cm^{-1} and at 1386 cm^{-1} attributed, respectively, to the asymmetric (ν_{as}) and symmetric (ν_s) stretching vibrations of COO^- groups, can be observed. The number of bands present in this spectral region suggests more than one coordination mode of carboxylate groups, what is in agreement with the structural description for $[Ln_2(BDC)_3(DMF)_2(H_2O)]$, (Ln = Eu, Gd). The

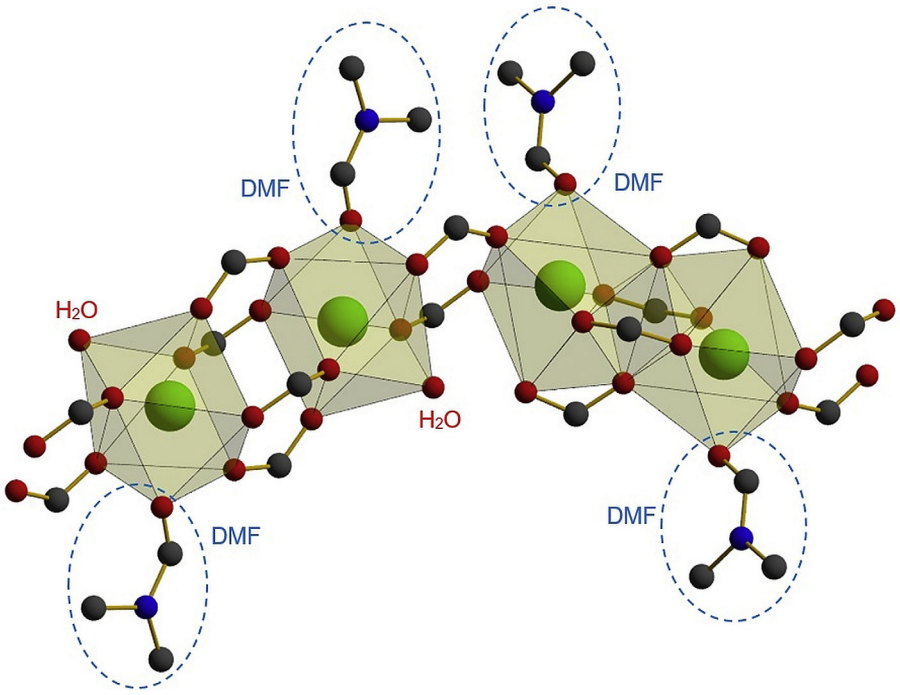

Fig. 2. Coordination environment of Eu^{3+} dimer in the crystal structure of Gd/Eu-MOF samples. Hydrogen atoms are omitted for clarity. Color code: gray (carbon), red (oxygen) and green (gadolinium or europium). (For interpretation of the references to colour in this figure legend, the reader is referred to the web version of this article.)

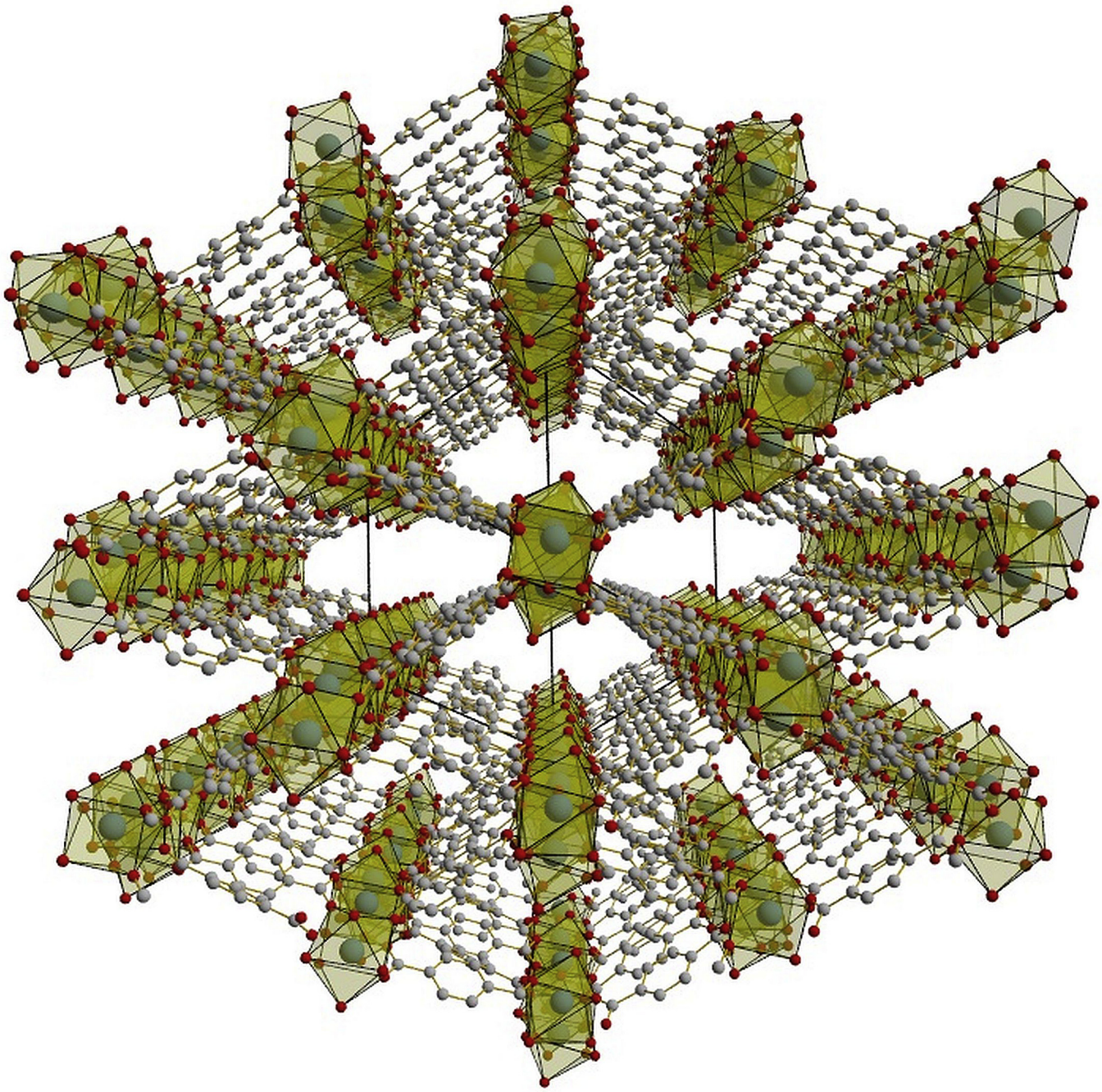

Fig. 3. Projection along the c axis of the partially expanded net structure of Gd/Eu-MOF samples. Hydrogen atoms and DMF molecules are omitted for clarity. Polyhedra in yellow represent the lanthanide sites. (For interpretation of the references to colour in this figure legend, the reader is referred to the web version of this article.)

difference between ν_{as} and ν_s, equal to $\Delta\nu = 152$ and 117 cm^{-1} might indicate a bidentate bridging and tridentate bridging-chelating coordination mode of carboxylates what was also found in the structure of $[Ln_2(BDC)_3(DMF)_2(H_2O)]$. A band around 1668 cm^{-1} may be attributed to the stretching ν (C═O) vibration of the coordinated DMF molecule. The band is slightly shifted compared to the stretching vibration ν (C═O) band of a free DMF (1657 cm^{-1}). Moreover, the δ (OCN) bending vibration band of DMF is shifted to higher frequencies compared to the absorption band of the pure DMF (from 659 to 676 cm^{-1}) confirming the presence of coordinated DMF molecule in all samples [25]. The broadband at around 3450 cm^{-1} can correspond to the water molecule present in the structure. The IR spectra of all samples also show bands in the region of 650–730 cm^{-1} and 500-620 cm^{-1} indicating the presence of coordinated water molecules. These data are in line with the crystal description for the reference sample $[Ln_2(BDC)_3(DMF)_2(H_2O)]$ for which coordinated solvent molecules H_2O and DMF were also found.

Thermogravimetric curves of the prepared Gd/Eu samples are shown in Fig. 5. The initial weight loss of 9.8% starting at around 100 °C up to 160 °C observed for all samples can be attributed to the loss of coordinated solvent molecules (DMF and H_2O). No mass loss

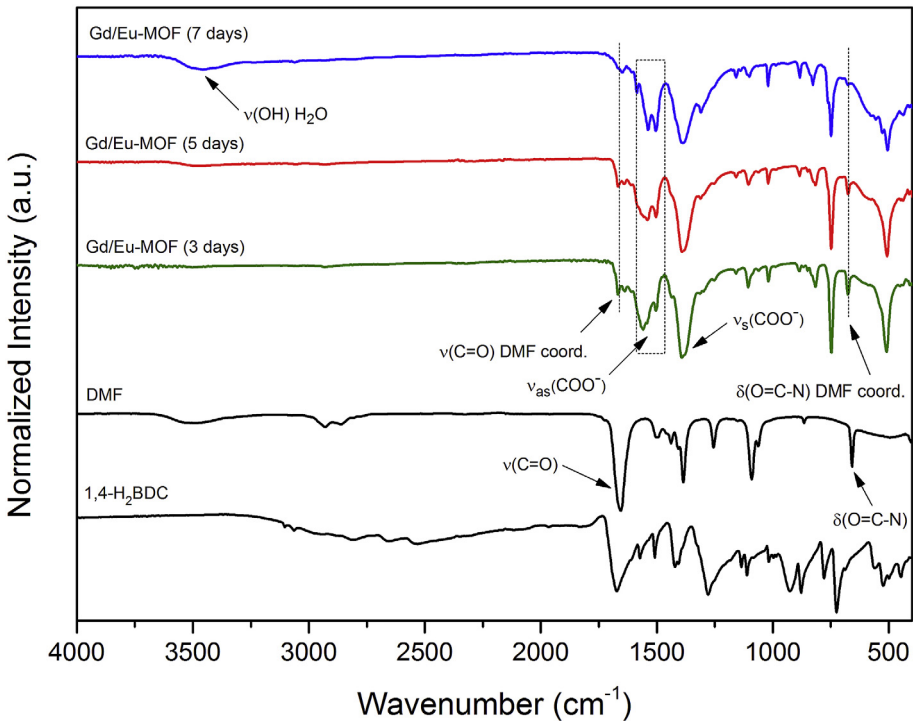

Fig. 4. FTIR spectra of the prepared Gd/Eu-MOF samples, the pure 1,4 − H_2BDC, and DMF.

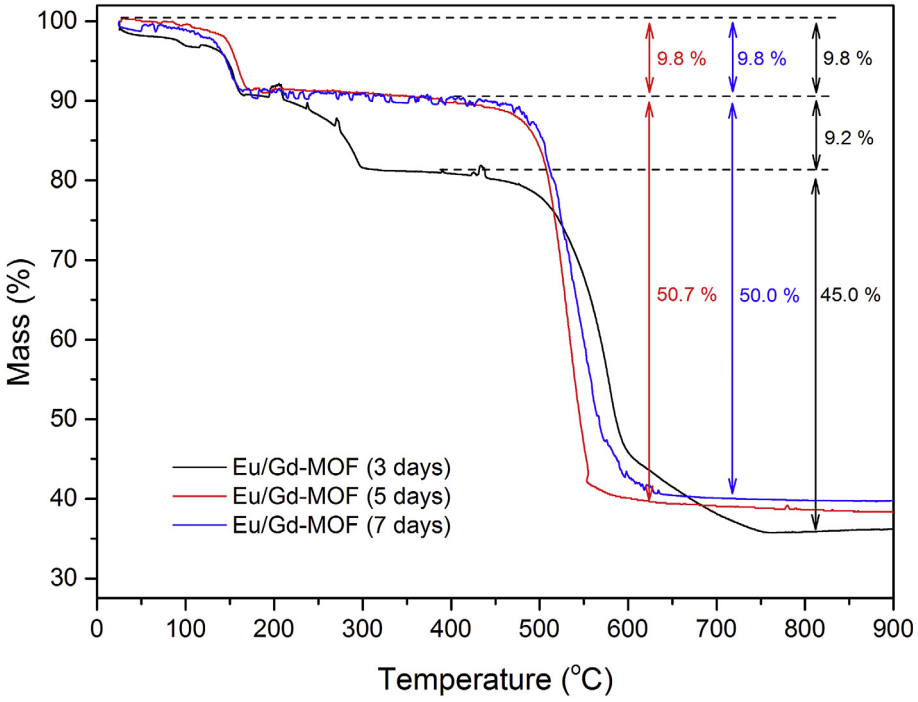

Fig. 5. TGA profiles of samples Gd/Eu-MOFs.

below 100 °C, commonly assigned to the desorption of solvent molecules from pores, is visible, what corroborates with XRD results.

For the sample prepared within the shortest synthesis time (3 days), the observed mass loss (9.2%) from 160 to 300 °C may be related to the decomposition of the unreacted ligand. The presence of an amorphous phase in the XRD diffraction pattern of this sample may also indicate the presence of the unreacted 1,4-H_2BDC. In all samples, the weight loss (45.0, 50.7 and 50.0%, respectively) starting from 650 °C is observed and can be attributed to the framework decomposition following the transformation into Gd and Eu oxides above 600 °C.

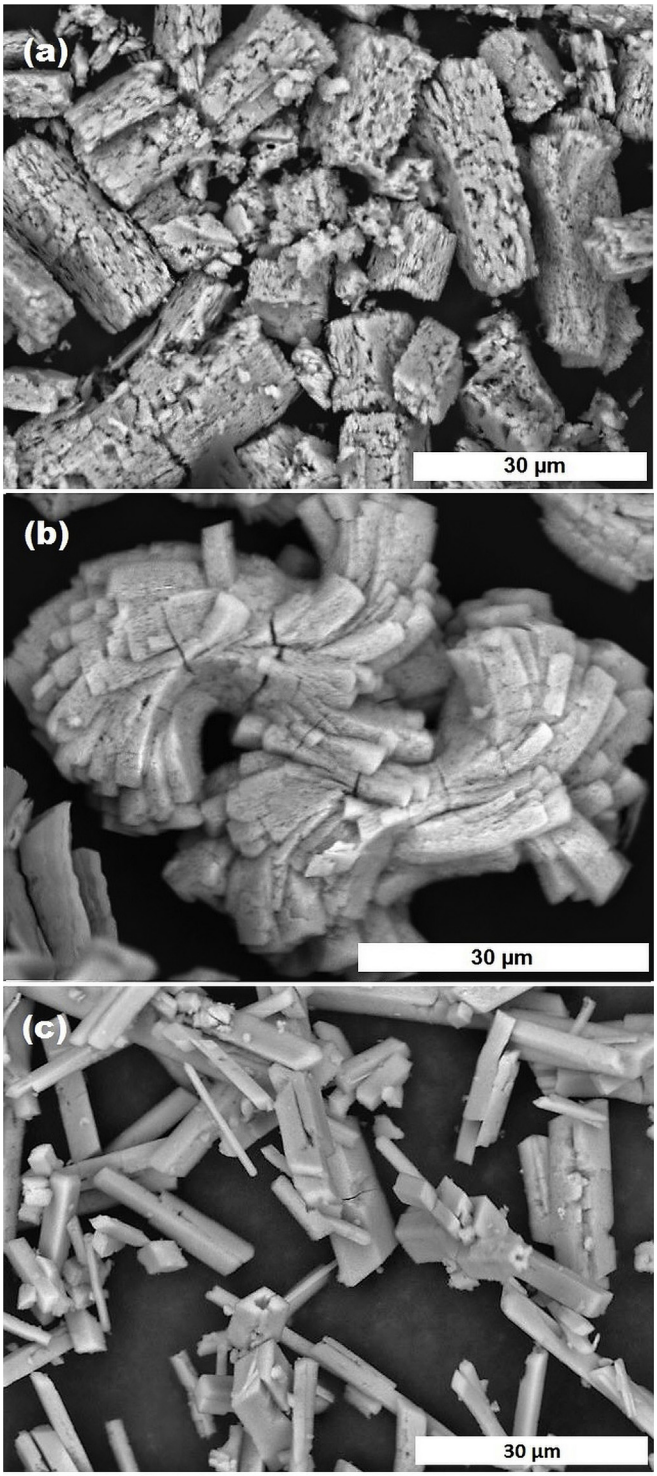

Fig. 6. SEM images of samples Gd/Eu-MOFs.

The morphology of the prepared powders was analyzed by SEM. As can be seen in Fig. 6a, the sample prepared within three days presents large porous microcrystals of the size around 30 μm. By increasing the synthesis time to five days, a decrease in porosity of the sample is observed (Fig. 6b). Finally, within seven days, apparently, pores disappear, and microcrystals with a rod-like shape are formed (Fig. 6c).

3.2. Photophysical properties

The photoluminescence excitation spectra of the samples prepared within 3, 5 and 7 days were recorded at room temperature by monitoring the transition $^5D_0 \rightarrow {}^7F_2$ at 614 nm (Fig. 7). The presence of the intense broadband with a maximum at 323 nm, corresponding to the $\pi \rightarrow \pi^*$ transitions of 1,4-BDC^{2-}, indicates an energy transfer from the ligand to the metal (antenna effect). The low-intensity narrow bands observed in the region of 350–550 nm are attributed to the 4f-4f transitions of Eu^{3+}. It is also worth to note that by increasing the synthesis time, the intensity of the transition $^7F_0 \rightarrow {}^5L_6$ of Eu^{3+} ion decreases, compared to the intensity of the broadband, what may be related with the crystallinity of the samples. These results suggest that the ligand-sensitized luminescence process (antenna effect) is more efficient than the direct excitation into the $^4F_6$ levels of the Eu^{3+} ion.

Crosby et al. have proposed a commonly accepted mechanism of the energy transfer from organic ligands to a lanthanide ion [26]. A ligand absorbs ultraviolet radiation and is excited to a vibrational level of the first excited singlet state (S0 → S1). The molecule undergoes fast internal conversion to lower vibrational levels of the S1 state, for instance through interactions with solvent molecules. The excited singlet state can undergo non-radiative intersystem crossing from the singlet state S1 to the triplet state T1. Subsequently, the system may undergo an intramolecular energy transfer from the triplet state to a level of the lanthanide ion.

Hilder and co-workers [27] have determined the energy level of the terephthalate triplet, 23.256 cm^{-1}, which is above the emission levels of the Eu^{3+} ion. This energy gap might cause numerous non-radiative relaxations before reaching the Eu^{3+} levels.

Recently, Decadt et al. have reported that the peaks corresponding to the 4f–4f transitions were comparable in intensity to the broadband originated from the ligand 1,4-BDC^{2-} in a Eu(III)-based MOF, and therefore concluded that the antenna effect was not very efficient [24].

On the other hand, our results show that the terephthalate ligand is a good sensitizer, and the efficient energy transfer observed in our case, may be related to the presence of the highly paramagnetic Gd^{3+} ions in the matrix [28]. The 4f levels of this ion are located above triplet levels of most organic ligands. Consequently, Gd^{3+}-centered emission cannot be observed. Moreover,

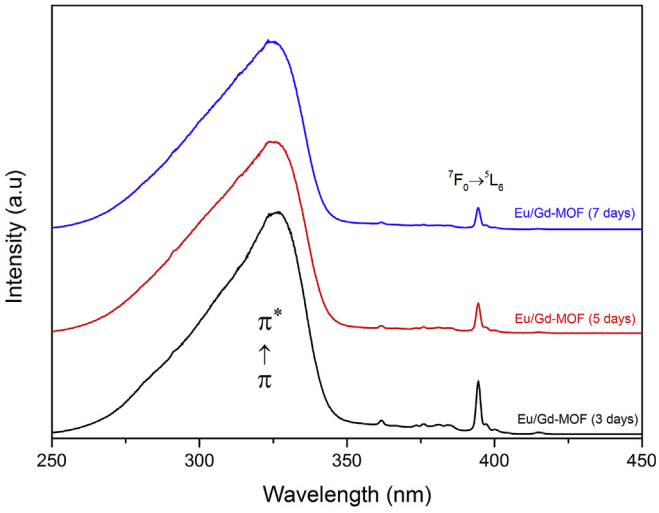

Fig. 7. Excitation spectra of samples Gd/Eu-MOFs measured at room temperature by monitoring the Eu^{3+} emission at 614 nm.

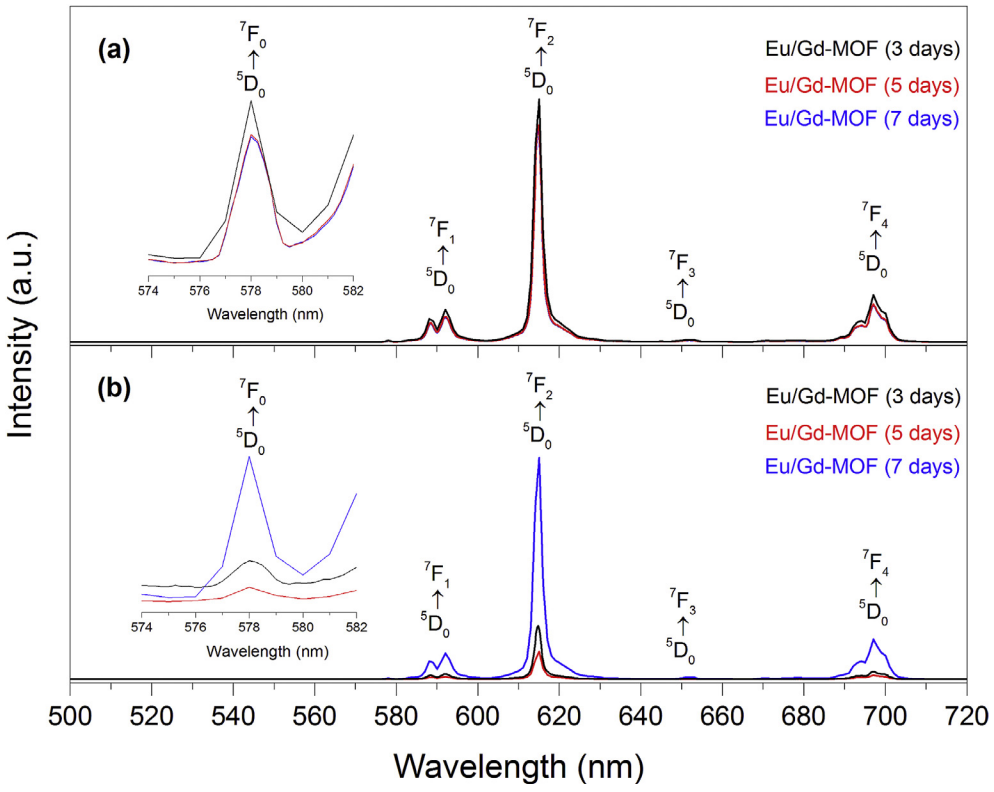

Fig. 8. Emission spectra of samples Gd/Eu-MOFs acquired at room temperature upon excitation at (a) 323 nm and (b) 395 nm.

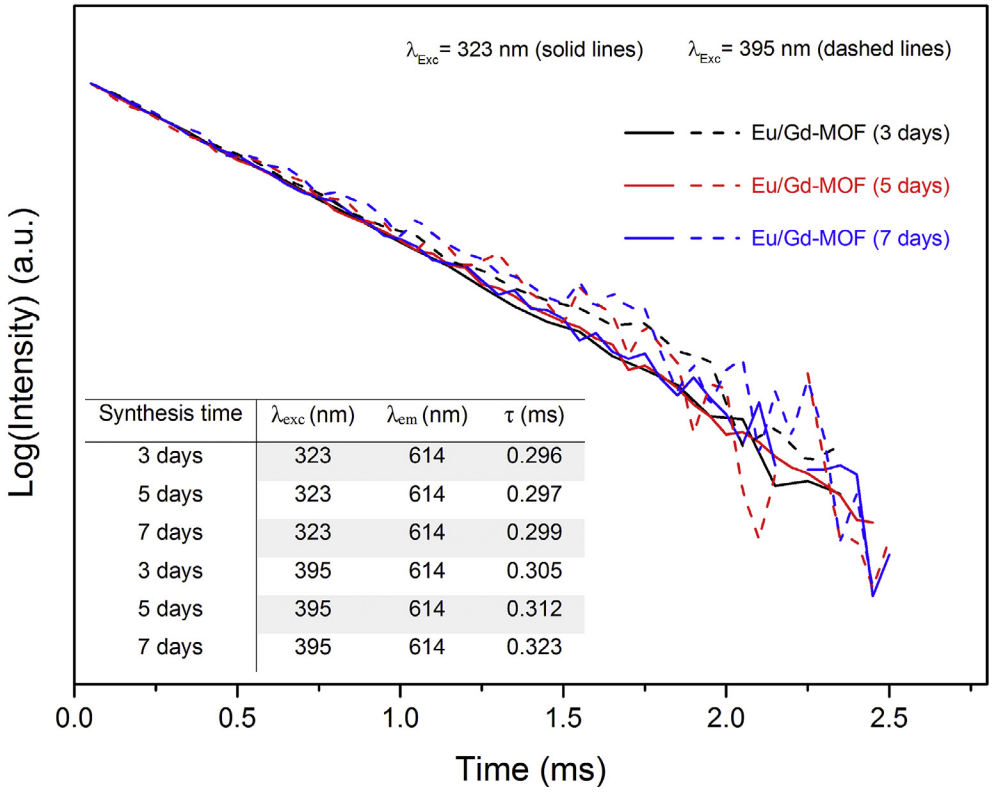

Synthesis time	λ_{exc} (nm)	λ_{em} (nm)	τ (ms)
3 days	323	614	0.296
5 days	323	614	0.297
7 days	323	614	0.299
3 days	395	614	0.305
5 days	395	614	0.312
7 days	395	614	0.323

Fig. 9. Luminescence decay emission curves obtained at room temperature upon excitation at 323 and 395 nm of samples Gd/Eu-MOFs. The inset table shows the values of decay lifetimes.

the presence of the heavy paramagnetic ion enhances the intersystem crossing (ISC) from the singlet (S1) to the triplet (T1) state because of mixing of the triplet and singlet states (paramagnetic effect) [29–31]. Although forbidden, this phenomenon occurs due to the spin-orbital coupling [32].

The emission spectra were recorded using two different excitation wavelengths ($\lambda_{ex} = 323$ and $\lambda_{ex} = 395$ nm) and are shown in Fig. 8. In both cases, only narrow and intense peaks assigned to the characteristic transitions of Eu^{3+} ($^5D_0 \rightarrow {}^7F_{0\text{-}4}$) are observed. The presence of the peak at 578 nm (see inset) corresponding to the strongly forbidden transition $^5D_0 \rightarrow {}^7F_0$ indicates that Eu^{3+} ions occupy a low symmetry site, without an inversion center such as C_{nv}, C_n or C_s [7]. The most intense peak with the maximum at 614 nm assigned to the electric dipole $^5D_0 \rightarrow {}^7F_2$ transition is responsible for the red luminescence of the prepared samples. The significant difference between peak intensities attributed to the $^5D_0 \rightarrow {}^7F_2$ and $^5D_0 \rightarrow {}^7F_1$ transitions, so called, the asymmetry factor, confirms the low-symmetry coordination environment around europium center [7,9]. These data are in good agreement with the results obtained from X-ray diffraction analysis. As previously presented in Fig. 2, Eu^{3+} and Gd^{3+} ions occupy sites with distorted square antiprism geometry, with low symmetry without an inversion center.

It is noteworthy to mention that the luminescence intensity is similar for all samples when excited at 323 nm (emission via energy transfer from the organic ligand to the Eu^{3+} levels). However, direct excitation of the Eu^{3+} ions at 395 nm ($^7F_0 \rightarrow {}^5L_6$ transition) causes the increase in the luminescence intensity of the sample prepared within 7 days compared to other samples, what might be associated with the different crystallinity of the samples.

The photoluminescence decay curves were obtained by monitoring the most intense emission at $\lambda_{em} = 614$ nm upon excitation in the ligand absorption level at 323 nm ($\pi \rightarrow \pi^*$) and upon direct excitation of the Eu^{3+} at 395 nm. The corresponding profiles are depicted in Fig. 9. The curves were found to fit a mono-exponential function what usually indicates the presence of only one coordination site of Eu^{3+} ions. However, as previously indicated by XRD data and as observed in Fig. 2, there are two different lanthanide sites in the crystal structure. Although uncommon, some crystal structures may have two slightly different sites with closely related time-dependent photoluminescence behavior [24]. In this case, a single exponential term can be used to fit the respective decay curve.

The photoluminescence decay times were measured at room temperature with excitation at 323 (organic ligand) and 395 nm (Eu^{3+}) and are shown in Fig. 9 (inset table). The values lie in the range of 0.296–0.299 and 0.305–0.323 ms, respectively. Compared to the reported values for europium terephthalate MOFs, which vary from 0.344 to 0.47 ms (hydrated) to 0.94 ms (anhydrous) [24], shorter decay times obtained in our case may confirm the presence of coordinated water molecules, as expected from the proposed crystal structure.

4. Conclusions

In summary, the synthesis and photophysical properties of intriguing bimetallic Gd-1,4-BDC MOFs doped with Eu^{3+} ions were presented here for the first time. Three syntheses carried out at different synthesis time (3, 5 or 7 days) were performed to evaluate the influence of the time of reaction on the microstructure, and consequently, the luminescent properties of such materials. In all samples, the Eu^{3+} ions were successfully incorporated in the Gd-1,4BDC MOF matrix without significant distortion of the matrix structure, what was confirmed by the XRD data analysis. The synthesis time, however, influenced the crystallinity of the prepared samples. It was observed that the sample prepared within 3 days presented very low crystallinity as a result of the short synthesis time and, moreover, the presence of the unreacted ligand was confirmed by the XRD and TGA analysis data. In the structure of Gd/Eu-1,4BDC MOF, two slightly different sites of Eu^{3+} ions were found, both octa-coordinated in a distorted square antiprism geometry. The results indicated that the ligand-sensitized luminescence process (antenna effect) is more efficient than the direct excitation into the $^4F_6$ levels of the Eu^{3+} ion. We suggested that the presence of highly paramagnetic Gd^{3+} ions enhanced the intersystem crossing (ISC) from the singlet (S1) to the triplet (T1) level and, as a consequence, also the antenna effect. Unlike excitation via antenna effect, the photoluminescence intensity observed upon direct excitation of the Eu^{3+} ions appeared to be dependent on the crystallinity of the samples. Further research concerning the relation structure/morphology – properties of Gd/EuMOFs is currently under investigation.

Acknowledgments

The authors thank Federal University of Pernambuco, School of Science and Technology/UFRN and Federal Institute of Education, Science and Technology of the Rio Grande do Norte (IFRN). This work was supported by CNPq (grant no. 407445/2013-7) and PRONEX/FACEPE/CNPq (grant no. APQ-0675- 1.06/14).

References

[1] A. Corma, H. Garcia, F.X. Llabrés i Xamena, Engineering metal organic frameworks for heterogeneous catalysis, Chem. Rev. 110 (2010) 4606–4655.
[2] G.S. Papaefstathiou, L.R. MacGillivray, Inverted metal–organic frameworks: solid-state hosts with modular functionality, Coord. Chem. Rev. 246 (2003) 169–184.
[3] Z. Bian, C. Huang, Electroluminescence based on lanthanide complexes, in: C. Huang (Ed.), Rare Earth Coordination Chemistry: Fundamentals and Applications, John Wiley & Sons (Asia) Pte Ltd, 2010, pp. 435–472.
[4] B.F. Hoskins, R. Robson, Infinite polymeric frameworks consisting of three dimensionally linked rod-like segments, J. Am. Chem. Soc. 111 (1989) 5962–5964.
[5] B.F. Abrahams, B.F. Hoskins, D.M. Michail, R. Robson, Assembly of porphyrin building blocks into network structures with large channels, Nature 369 (1994) 727–729.
[6] H. Li, M. Eddaoudi, M. O'Keeffe, O.M. Yaghi, Design and synthesis of an exceptionally stable and highly porous metal-organic framework, Nature 402 (1999) 276–279.
[7] B. Chen, L. Wang, Y. Xiao, F.R. Fronczek, M. Xue, Y. Cui, G. Qian, A luminescent metal–organic framework with Lewis basic pyridyl sites for the sensing of metal ions, Angew. Chem. Int. Ed. 48 (2009) 500–503.
[8] L. Yang, S. Zhang, X. Qu, Q. Yang, X. Liu, Q. Wei, S. Chen, Synthesis, crystal structure and photoluminescence property of Eu/Tb MOFs with mixed polycarboxylate ligands, J. Solid State Chem. 231 (2015) 223–229.
[9] B.V. Harbuzaru, A. Corma, F. Rey, P. Atienzar, J.L. Jordá, H. García, J. Rocha, Metal–organic nanoporous structures with anisotropic photoluminescence and magnetic properties and their use as sensors, Angew. Chem. Int. Ed. 47 (2008) 1080–1083.
[10] F. Pellé, P. Aschehoug, S. Surblé, F. Millange, C. Serre, G. Férey, Interactions between Eu3+ ions in inorganic–organic hybrid materials, J. Solid State Chem. 183 (2010) 795–802.
[11] K.M. Taylor, A. Jin, W. Lin, Surfactant-assisted synthesis of nanoscale gadolinium metal–organic frameworks for potential multimodal imaging, Angew. Chem. 120 (2008) 7836–7839.
[12] J. Lee, O.K. Farha, J. Roberts, K.A. Scheidt, S.T. Nguyen, J.T. Hupp, Metal–organic framework materials as catalysts, Chem. Soc. Rev. 38 (2009) 1450–1459.
[13] C.Y. Sun, C. Qin, X.L. Wang, Z.M. Su, Metal-organic frameworks as potential drug delivery systems, Expert Opin. Drug Deliv. 10 (2013) 89–101.
[14] B.S. Barros, J. Chojnacki, A.A.M. Soares, J. Kulesza, L.L. da Luz, S.A. Júnior, Thermostability and photophysical properties of mixed-ligand carboxylate/benzimidazole Zn (II)-coordination polymers, Mat. Chem. Phys. 162 (2015) 364–371.
[15] I.T. Weber, A.J.G. de Melo, M.A.D.M. Lucena, M.O. Rodrigues, S.A. Júnior, High photoluminescent metal–organic frameworks as optical markers for the identification of gunshot residues, Anal. Chem. 83 (2011) 4720–4723.
[16] I.T. Weber, I.A. Terra, A.J. de Melo, M.A.D.M. Lucena, K.A. Wanderley, C.D.O. Paiva-Santos, S.A. Júnior, Up-conversion properties of lanthanide-organic frameworks and how to track ammunitions using these materials, Rsc Adv. 2 (2012) 3083–3087.

[17] F.A.A. Paz, J. Klinowski, S.M. Vilela, J.P. Tome, J.A. Cavaleiro, J. Rocha, Ligand design for functional metal–organic frameworks, Chem. Soc. Rev. 41 (2012) 1088–1110.
[18] R.E. Morris, Ionothermal synthesis—ionic liquids as functional solvents in the preparation of crystalline materials, Chem. Commun. 21 (2009) 2990–2998.
[19] X.P. Yang, R.A. Jones, J.H. Rivers, R.P.J. Lai, Syntheses, structures and luminescent properties of new lanthanide-based coordination polymers based on 1,4-benzenedicarboxylate (bdc), Dalton T 35 (2007) 3936–3942.
[20] T.M. Reineke, M. Eddaoudi, M. Fehr, D. Kelley, O.M. Yaghi, From condensed lanthanide coordination solids to microporous frameworks having accessible metal sites, J. Am. Chem. Soc. 121 (1999) 1651–1657.
[21] A. Deluzet, W. Maudez, C. Daiguebonne, O. Guillou, Interplane distances modulation in lanthanide-based coordination polymers, Cryst. Growth Des. 3 (2003) 475–479.
[22] L. Pan, N. Zheng, Y. Wu, S. Han, R. Yang, X. Huang, J. Li, Synthesis, characterization and structural transformation of a condensed rare earth metal coordination polymer, Inorg. Chem. 40 (2001) 828–830.
[23] X. Guo, G. Zhu, F. Sun, Z. Li, X. Zhao, X. Li, S. Qiu, Synthesis, structure, and luminescent properties of microporous lanthanide metal-organic frameworks with inorganic rod-shaped building units, Inorg. Chem. 45 (2006) 2581–2587.
[24] R. Decadt, K. Van Hecke, D. Depla, K. Leus, D. Weinberger, I. Van Driessche, R. Van Deun, Synthesis, crystal structures, and luminescence properties of carboxylate based rare-earth coordination polymers, Inorg. Chem. 51 (2012) 11623–11634.
[25] S. Akopyan, H. Bertagnolli, I. Boyarskaya, D. Leicht, R. Merkle, L. Solovieva, E. Vilaseca, IR spectra and microstructure of electrolyte solutions. Dependence of spectroscopic characteristics of solvated molecules on composition of solvates in the system CH3CN–$Mg(ClO_4)$ 2–DMF, Phys. Chem. Chem. Phys. 3 (2001) 2098–2104.
[26] G.A. Crosby, R.E. Whan, J.J. Freeman, Spectroscopic studies of rare earth chelates, J. Phys. Chem. 66 (1962) 2493–2499.
[27] M. Hilder, P.C. Junk, U.H. Kynast, M.M. Lezhnina, Spectroscopic properties of lanthanoid benzene carboxylates in the solid state: Part 1, J. Photochem. Photobiol. 202 (2009) 10–20.
[28] L. Liao, C.W. Ingram, D. Vandeveer, K. Hardcastle, K.M. Solntsev, D. Sabo, R.T. Weber, Poly-(bis ((μ 4-1, 4-benzenedicarboxylato)-bis (μ 2-N, N-dimethylformamide)-(nitrato)-gadolinium (III))) metal organic framework: synthesis, magnetic and luminescence properties, Inorg. Chim. Acta 391 (2012) 1–9.
[29] K. Binnemans, Lanthanide-based luminescent hybrid materials, Chem. Rev. 109 (2009) 4283–4374.
[30] S. Tobita, M. Arakawa, I. Tanaka, Electronic relaxation processes of rare earth chelates of benzoyltrifluoroacetone, J. Phys. Chem. 88 (1984) 2697–2702.
[31] S. Tobita, M. Arakawa, I. Tanaka, The paramagnetic metal effect on the ligand localized S1 →T1 intersystem crossing in the rare-earth-metal complexes with methyl salicylate, J. Phys. Chem. 89 (1985) 5649–5654.
[32] S.P. McGlynn, T. Azumi, M. Kinoshita, Molecular Spectroscopy of the Triplet State, Prentice-Hall, 1969.